Prediction of Channel Excess Attenuation for Satellite Communication Systems at Q-Band Using Artificial Neural Network

Prediction of Channel Excess Attenuation for Satellite Communication Systems at Q-band Using Artificial Neural Network

Lu Bai, Cheng-Xiang Wang, *Fellow, IEEE*, Qian Xu, and Spiros Ventouras, George Goussetis, *Senior Member, IEEE*

Abstract—This paper proposes the use of an artificial neural network (ANN) for estimating the fading of a Q-band (39.402 GHz) satellite channel exploiting knowledge of its previous state as well as the present weather conditions. The ANN is trained using weather data and propagation measurements at Q-band obtained during a period of nine months by the Aldo Paraboni receivers of RAL Space at Chilbolton. Subsequently, the estimation obtained by the ANN is compared with actual propagation measurements on data obtained over a period of three months. Statistical analysis demonstrates agreement between the ANN estimation and the measurement within a 1 dB range with a probability exceeding 98.8%. The significance of this work lies with the opportunities it raises to deliver real-time fading estimations using low-cost weather sensors combined with feedback on the channel state from the return link, which can be used in the deployment of propagation impairment mitigation techniques (PIMTs).

Index Terms—Satellite communication systems, channel excess attenuation, artificial neural network, weather conditions.

I. INTRODUCTION

The role of satellite communications in emerging wireless communication systems stems from their capability to deliver worldwide broadband coverage [1]. While traditional satellite services have relied on C- and Ku-bands, the transition from broadcast to broadband services and the ever increasing need for higher bandwidth at reduced costs drives the exploitation of higher millimeter wave (mmW) bands. Currently, the use of Q/V-band for the feeder link of satellite communication systems is being rolled out as means to free Ka-band spectrum

L. Bai is with Shandong Provincial Key Lab of Wireless Communication Technologies, School of Information Science and Engineering, Shandong Unviersity, Qingdao, 266237, Shandong, China (e-mail: bailusdu@126.com).

C.-X. Wang (corresponding author) and G. Goussetis are with the Institute of Sensors, Signals and Systems, School of Engineering and Physical Sciences, Heriot-Watt University, Edinburgh, EH14 4AS, U.K. C.-X. Wang is also with the National Mobile Communications Research Laboratory, School of Information Science and Engineering, Southeast University, Nanjing 210096, China, and with the Purple Mountain Laboratories, Nanjing 211111, China (e-mail: chxwang@seu.edu.cn, g.goussetis@hw.ac.uk).

Q. Xu is with School of Computer Science and Technology, Jilin University, Changchun, Jilin, 130012, China (e-mail: quincyxu@hotmail.com).

S. Ventouras is with STFC Rutherford Appleton Laboratory, RAL Space, Oxford, OX11 0QX, U.K. (e-mail: spiros.ventouras@stfc.ac.uk).

to revenue generating user links and reduce the per bit cost of the ground segment [2].

Despite aforementioned advantages, atmospheric fading at Q/V-band is significantly higher compared to that at C-band or Ku-band. Consequently, the traditional approach of allowing for a sufficiently high margin in the link budget is no longer efficient within the existing technology base. Instead, alternative fade mitigation techniques are preferred, such as adaptive coding and modulation and dynamic power control [3], [4]. Critically, the efficient deployment of these techniques relies on accurate real-time knowledge of the channel fading that will enable the optimum reconfiguration of link parameters such as the modulation and coding rate, or the power amplifier's input backoff [5], [6].

The existing models of channel impairments can be classified into deterministic models, empirical models, and stochastic models [7], [8]. Deterministic models [9]–[12] are generated using ray-tracing techniques which determine the transmission mechanism and path of electromagnetic wave. They are accurate but complex and not flexible. Empirical models [13]–[15] are directly generated by fitting curves with measurement data. They are easy-to-use but but cannot represent the propagation features of physical channels. Stochastic models are established with certain [17] or mixed distributions [18], or even different states represented using Markov chains [19], such as Suzuki model [20], Loo's model [21], and Lutz's model [22]. They can achieve a good trade-off between accuracy and generality. Besides, International telecommunication union offers a series of documents to calculate free-space attenuation, atmospheric gases attenuation, rain attenuation, clouds and fog attenuation, and ionospheric attenuation. However, they are accurate but too complex [23]–[27].

Aforementioned models were generated by conventional channel modeling methods. They can describe channel characteristics but cannot accurately predict the received signal attenuation in a certain time resulting from channel impairments. Recently, articial neural network (ANN) widely used in various research areas has good performance on certain prediction [28], [29]. In principle, the channel state information (CSI) for broadband services can be reported to the gateway by virtue of the return link. However the non-negligible latency associated with the combined forward and return links impose a delay in the knowledge of the CSI. Additional instrumentation should then be deployed in order to enable real time estimation of the fading. This includes spaceborne beacons with associated

ground receivers or radiometers, which provide a calibrated reading of the atmosphere's brightness temperature. However these provisions add a non-negligible value to the overall costs.

Addressing aforementioned needs, this contribution proposes a cost-efficient methodology to obtain real-time estimation of the atmospheric fading. The proposed approach exploits an ANN which takes as input earlier fading values, which can be obtained from the return link, as well as present weather information, which can be obtained with low-cost weather stations. Exploiting Q-band propagation and weather data obtained during a period of one year by the RAL Space Aldo Paraboni receiver station in Chilbolton [30], we demonstrate that once training has been undertaken, the ANN can then provide an accurate estimation of the real-time fading.

II. SYSTEM MODEL

The flowchart of the ANN enabled approach we adopted for predicting channel excess attenuation associated with a satellite link is shown in Fig. 1. Exploiting the Aldo Paraboni Q-band beacon, we firstly record the excess attenuation associated with the channel. Together we also record local weather conditions. The data is then split into three datasets, for training, validation and testing respectively. We used data recorded over a period of one year and split them in the three datasets following a proportion of 2:1:1. The training dataset and validation dataset, both containing input and output vectors, are used to train the network for the parameter selection and configuration of the neural network [31]. When the training process is finished, the input vectors of test dataset are put into the trained ANN to get predicted channel excess attenuation. The predicted performance of the trained ANN is evaluated by comparing the predicted channel excess attenuation and the output vectors of test dataset (i.e. the true measured value).

The architecture of the proposed ANN for predicting the channel excess attenuation is presented in Fig. 2. The output vector Y is the present channel excess attenuation h. In order to evaluate the significance of each input parameter, we explore four different variations of the input vectors, i.e., X_1, X_2, X_3, and X_4, which can be expressed as

$$X_1 = [\alpha, \beta, \gamma, \vartheta, \varphi] \tag{1}$$

$$X_2 = [\alpha, \beta, \gamma, \vartheta, \varphi, h'] \tag{2}$$

$$X_3 = [\alpha, \beta, \gamma, \vartheta, \varphi, \varepsilon, \kappa] \tag{3}$$

$$X_4 = [\alpha, \beta, \gamma, \vartheta, \varphi, \varepsilon, \kappa, h'] \tag{4}$$

$$Y = [h] \tag{5}$$

where $\alpha, \beta, \gamma, \vartheta, \varphi, \varepsilon, \kappa$ are the present value for air temperature, relative humidity, rainfall rate, visibility, thickness of rainfall amount, average particle diameter, and average particle speed, h' is the channel excess attenuation in the previous one minute.

The vector X_1 consists of five typical parameters of current weather conditions that can be obtained with low-cost standard instrumentation, namely: air temperature, relative humidity, rainfall rate, visibility, and thickness of rainfall amount. The variable X_3 includes two further parameters that would require
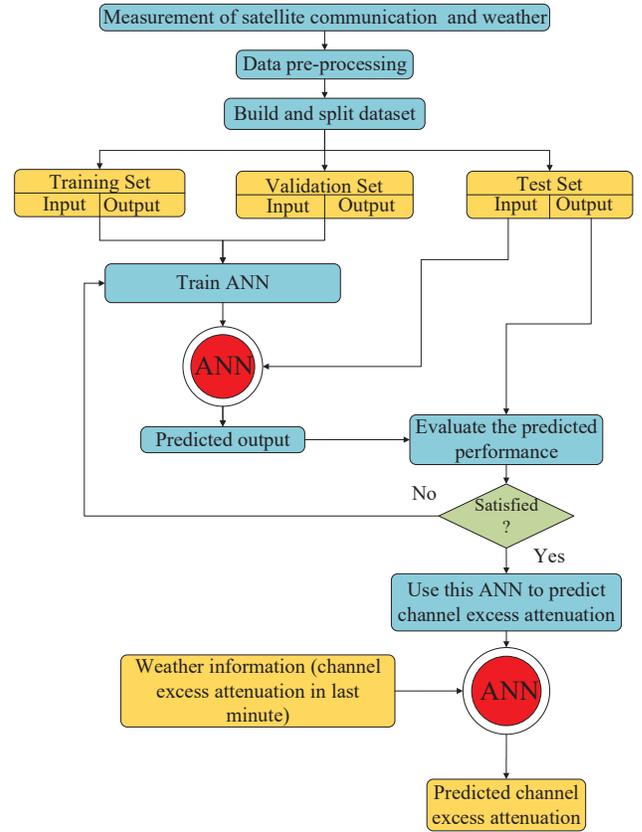

Fig. 1. The flowchart of channel excess attenuation predicting procedure.
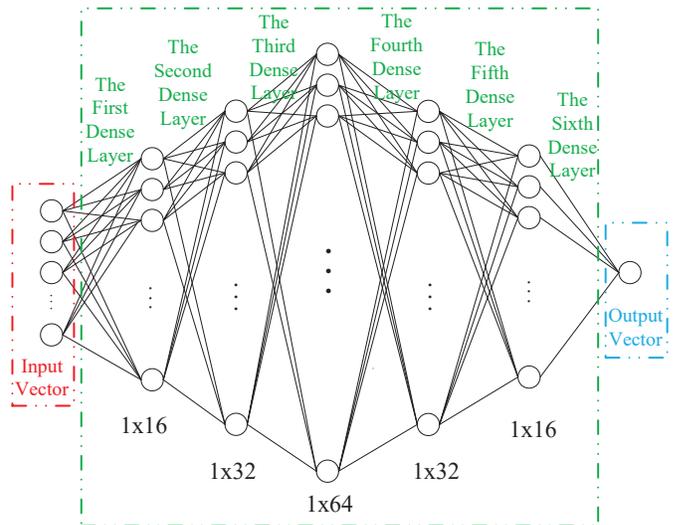

Fig. 2. The architecture of the proposed ANN for channel excess attenuation prediction.

TABLE I
THE NUMBERS AND PERCENTAGES OF PARAMETERS OF FOUR MODELS.

Layers	A model $X_1 \rightarrow Y$		B model $X_2 \rightarrow Y$		C model $X_3 \rightarrow Y$		D model $X_4 \rightarrow Y$	
	Number	Percentage	Number	Percentage	Number	Percentage	Number	Percentage
First dense layer	80	1.53%	96	1.83%	112	2.13%	128	2.43%
Second dense layer	512	9.82%	512	9.79%	512	9.76%	512	9.73%
Third dense layer	2048	39.26%	2048	39.14%	2048	39.02%	2048	38.91%
Fourth dense layer	2048	39.26%	2048	39.14%	2048	39.02%	2048	38.91%
Fifth dense layer	512	9.82%	512	9.79%	512	9.76%	512	9.73%
Sixth dense layer	16	0.31%	16	0.31%	16	0.30%	16	0.30%
Total	5216		5232		5248		5264	

TABLE II
THE MEANS, STANDARD DEVIATIONS, AND PCC BETWEEN
MEASUREMENT DATA AND PREDICTED DATA BY X_1, X_2, X_3, AND X_4.

	Mean	Standard Deviation	Correlation Coefficient
Measurement	0.4041	1.2338	1
X1	0.4007	0.9477	0.761
X2	0.4079	1.211	0.9549
X3	0.4028	0.914	0.7696
X4	0.412	1.2075	0.9549

the deployment of an additional instrument, a disdrometer, namely: average particle diameter and average particle speed. The comparison between the predicted performance obtained from X_1 and X_3 is meaningful to analyze the significance of deploying a disdrometer. The variables X_2 and X_4 add the channel excess attenuation recorded in the previous one minute on X_1 and X_3, which can be obtained exploiting the return link.

After testing kinds of ANN architectures and adjusting the architecture parameters of above ANNs, such as the learning rate, mini batch, epochs, loss function and so on, The ANN we employed is a multi-layer perceptron which is composed of six dense layers. The six dense layers have 16, 32, 64, 32, 16, and 1 neurons, respectively. Its architecture is shown in Fig. 2. Through iterations using the training dataset, the neural network converges to fit the thresholds, nodes and weights of connections for the least loss. As shown in Table I, the four model A–D whose input vectors are X_1, X_2, X_3, and X_4, has 5216, 5232, 5248 and 5264 parameters in total, respectively. The third and fourth dense layers have the majority of model parameters, which account for approximately 80% of the total number of model parameters. The loss function is a quantification to evaluate how good a prediction model is in terms of predicting the expected outcome. The mean square error (MSE), which is expressed as R, is the most commonly used regression loss function and easy-to-use in our multi-layer perceptron. It is the average value of squared distances between our target variable and predicted values, and can be expressed as

$$R = \frac{\sum_{n=1}^{N}(y_n - y_n^{\mathrm{p}})^2}{N} \tag{6}$$

where N denotes the data numbers of dataset, y_n and y_n^{p} are true value and predicted value, respectively.

The learning rates for all the dense layers were initialized at 0.0001. The root-mean-square propagation (RMSProp) is used to optimize the weights of our multi-layer perceptron with the smooth factor of 10^{-6} and the momentum of 0.9. The update rule for weight β is defined as

$$E[g^2]_t = 0.9E[g^2]_{t-1} + 0.1g_t^2 \tag{7}$$

$$\beta_{t+1} = \beta_t - \frac{\eta}{\sqrt{E[g^2]_t + \kappa}}g_t \tag{8}$$

where t, η, and κ denote the iteration index, the learning rate, and the smooth factor, respectively, g_t is the gradient of the current iteration t [31] [32].

The Xavier uniform initializer, which is also recognized as the Glorot uniform initializer, is applied to initialize the weights in each layer [33]. The weight was generated with a uniform distribution randomly within $[-\varepsilon, \varepsilon]$ where

$$\varepsilon = \sqrt{\frac{6}{\iota_{in} + \iota_{out}}} \tag{9}$$

where ι_{in} and ι_{out} are the numbers of input units and output units in the weight tensor. The neuron biases in dense layers is initialized with the constant 0. The rectified linear units (ReLU) in our multi-layer perceptron are provided positive inputs to accelerate the early stages of learning.
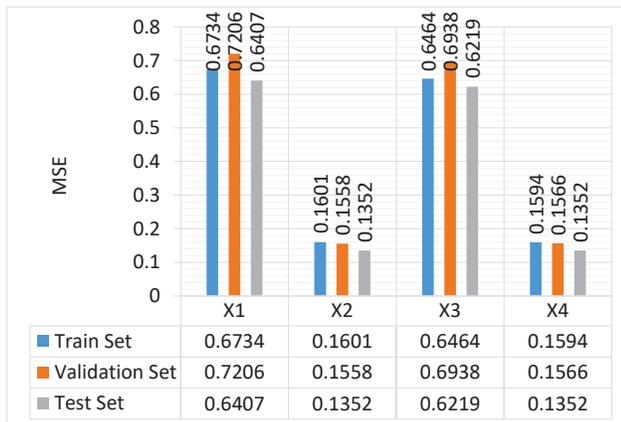
III. RESULTS AND ANALYSIS

A. Data collection

A series of radio propagation measurements at Q-band (39.402 GHz) in Chilbolton, Hampshire, UK are carried out using the Aldo Paradoni Payload propagation beacon [30]. The weather condition data is collected by the Chilbolton Facility for Atmospheric and Radio Research (CFARR) Campbell Scientific PWS100 present weather sensor in Chilbolton, Hampshire, UK. The instrument is mounted approximately 10 m above ground on the roof of a cabin at the Chilbolton Observatory site. We take the radio propagation measurement data and weather condition data from 1st Jan. 2017– 31st Dec. 2017. For the trade-off between accuracy and complexity, the received signal and parameters of weather conditions are sampled by 1/60 Hz. The excess attenuation is calculated based on the received signal [30].

B. Comparison in the time domain

In Fig. 3(a), a total of 3000 samples of measurement data and predicted data by input vectors X_1, X_2, X_3, and X_4 are shown. As observed, the predicted data follows well the trends of the channel excess attenuation, thus qualitatively confirming the predicting ability of the proposed method.

Fig. 3(b), which is a zoom in version of the selected red part of Fig. 3(a), compares the performance when the four different input vectors are used. There are 12 significant peaks which are meaningful to be predicted in the 150 samples shown in Fig. 3(b). The prediction by input vectors X_2 and X_4, which has the channel excess attenuation in the previous one minute as the input vector, can predict all 12 peaks in 150 samples.

TABLE III
THE MSEs OF PREDICTED DATA BY X_1, X_2, X_3, AND X_4 IN THREE SETS.

	X1	X2	X3	X4
Train Set	0.6734	0.1601	0.6464	0.1594
Validation Set	0.7206	0.1558	0.6938	0.1566
Test Set	0.6407	0.1352	0.6219	0.1352

The prediction by input vectors X_1 and X_3, which only has the weather conditions as input vector, cannot predict the variation of channel extenuation at peak 5, 6, and 7. Moreover, the predictions by input vectors X_1 and X_3 at peak 4, 8, and 10 are lower than the measurement data, not as accurate as those obtained from input vectors X_2 and X_4.

C. Statistical analysis

In order to quantify the performance of the proposed method, next we present statistical analysis of the predicted results vs the actual measured results. The means, standard deviations, and Pearson product-moment correlation coefficient (PCC) between measurement data and predicted data are given in Table II. The means of predicted data by four different input vectors are roughly equal with the mean of measurement data. However, their standard deviations show some significant statistical differences. The standard deviations of predictions by input vectors X_2 and X_4, which have the channel excess attenuation in the previous one minute as input vector, are closer with that of measurement data. The PCC between the measurement data and the predicted data by input vectors X_2 and X_4 are both 0.9549, nearly to 1, which shows their effectiveness. Instead, the PCC between measurement data and predicted data by input vectors X_1 and X_3 are much lower.

The MSE of predicted data for the train set, validation set, and test set are presented in Table III. The MSE trends in the three datasets are relatively stable, which demonstrate the validation and stationarity of our ANN. The MSEs of predictions by input vectors X_2 and X_4 are much lower than those of predictions by input vectors X_1 and X_3. The cumulative distribution functions (CDFs) of the absolute error of predicted data against the measured ones are shown in Fig. 4. Compared with predictions by input vectors X_1 and X_3, the CDFs of absolute error of predicted data by X_2 and X_4 are much higher and with a faster rise. The percentages of absolute error within 1dB by both X_1 and X_3 are above 90%. Adding the channel attenuation in the previous one minute as input (X_2 and X_4), the percentage of absolute error within 1dB is 98.85%. The CDF of the absolute error of predicted data by X_1 is very similar with the CDF of absolute error of predicted data by X_3, which suggests that the additional

weather data associated with a disdrometer is not particularly helpful for predicting the fading.

IV. CONCLUSIONS

In this paper, we have proposed a method of estimating channel excess attenuation in mmW satellite links using ANN. The data used to train the ANN were obtained by measurement campaigns of local weather conditions and satellite communication signal by Alphasat beacon receiver at Q-band in Chilbolton, Hampshire, UK. By analyzing time series as well as statistical characteristics obtained by the proposed ANN against the measured data, we have demonstrated that it is possible to obtain very accurate estimations of the channel excess attenuation using information obtained from low-cost weather instrumentation and CSI from the return link, especially the CDF of absolute error between the ANN estimation and the measurement within a 1 dB range is with a probability exceeding 98.8%. We also found predictions which have the channel excess attenuation in last minute as input vector obtain better performance significantly and predictions which have more two parameters of weather information as input vector obtain better performance slightly. The proposed methodology can thus provide pertinent pathways for the efficient and low-cost deployment of propagation impairment mitigation techniques such as adaptive coding and modulation and dynamic power control.

REFERENCES

[1] 3GPP, TR 38.811, "Study on new radio (NR) to support non terrestrial networks," Dec. 2017.
[2] H. Fenech, A. Tomatis, S. Amos, J. S. Merino, and V. Soumpholphakdy, "An operator's perspective on propagation," in *Proc. IEEE EUCAP'14*, The Hague, Netherlands, Apr. 2014, pp. 2164–3342.
[3] ETSI EN 302 307-2 v1.1.1 (2014-10), "Digital Video Broadcasting (DVB); Second generation framing structure, channel coding and modulation systems for broadcasting, interactive services, news gathering and other broadband satellite applications; Part 2: DVB Extensions (DVB-S2X)".
[4] E. Casini, R. De Gaudenzi, and A. Ginesi, "DVB-S2 modem algorithms design and performance over typical satellite channels," *Int. J. Satell. Commun. Network.*, vol. 22, pp. 281–318, Jun. 2004.
[5] G. Karam and H. Sari, "A data pre-distortion technique with memory for QAM radio systems," *IEEE Trans. Commun.*, vol. 39 no. 2, pp. 336–344, Feb. 1991.
[6] B. Li, C. Zhao, M. Sun, H. Zhang, Z. Zhou, A. Nallanathan, "A Bayesian approach for nonlinear equalization and signal detection in millimeter-wave communications," *IEEE Trans. Wireless Commun.*, vol. 14, no. 7, pp. 3794–3809, Jul. 2015.
[7] C.-X. Wang, J. Bian, J. Sun, W. Zhang, and M. Zhang, "A survey of 5G channel measurements and models," *IEEE Commun. Surveys Tuts.*, vol. 20, no. 4, pp. 3142–168, 4th Quart., 2018.
[8] S. Wu, C.-X. Wang, H. Aggoune, M. M. Alwakeel, and X. You, "A general 3D non-stationary 5G wireless channel model," *IEEE Trans. Commun.*, vol. 66, no. 7, pp. 3065–3078, July 2018.
[9] M. Dottling, H. Ernst, and W. Wiesbeck, "A new wideband model for the land mobile satellite propagation channel," in *Proc. IEEE ICUPC'98*, Florence, Italy, Oct. 1998, pp. 647–651.
[10] M. Dottling, A. Jahn, and W. Wiesbeck, "A comparison and verification of 2D and 3D ray tracing propagation. models for land mobile satellite communications," in *Proc. IEEE APSIS'00*, Salt Lake City, USA, Jul. 2000, pp. 434–437.
[11] T. Sofos, I. Koutsopoulos, and P. Constantinou, "A deterministic raytracing based model for land mobile satellite channel in urban environment," in *Proc. IEEE VTC'98*, Ottawa, Canada, May 1998, pp. 658–660.
[12] C. Oestges, S. R. Saunders and D. Janvier, "Physical statistical modelling of the land mobile satellite channel based on ray tracing," *IEE Proceedings - Microwaves, Antennas and Propagation*, vol. 146, no. 1, pp. 45–49, Feb. 1999.
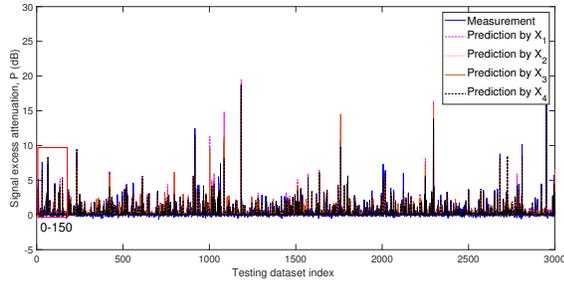
(a) 3000 samples of measurement data and predicted data.
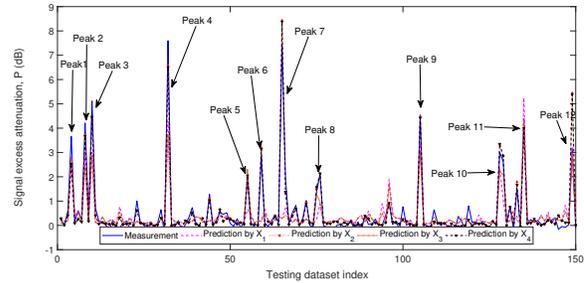
(b) 150 samples of measurement data and predicted data.

Fig. 3. The time series of measurement data and predicted data by X_1, X_2, X_3, and X_4.
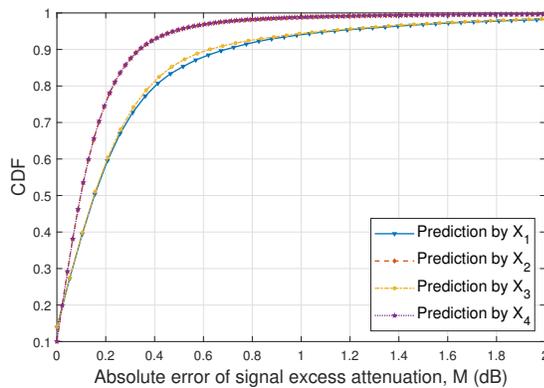

Fig. 4. The CDFs of absolute error of predicted data by X_1, X_2, X_3, and X_4.

[13] W. Vogel and J. Goldhirsh, "Earth-satellite tree attenuation at 20 GHz: foliage effects," *Electronics Lett.*, vol. 29, no. 18, pp. 1640–1641, Sept. 1993.

[14] W. Vogel and J. Goldhirsh, "Mobile satellite system propagation measurements at L-band using marecs-b2," *IEEE Trans. Antennas Propag.*, vol. 38, no. 2, pp. 259–264, Feb. 1990.

[15] E. Cid, A. V. Alejos and M. G. Sanchez, "Signaling through scattered vegetation: empirical loss modeling for low elevation angle satellite paths obstructed by isolated thin trees," *IEEE Trans. Veh. Technol. Mag.*, vol. 11, no. 3, pp. 22–28, Sept. 2016.

[16] A. Kanatas and P. Constantinou, "City center high-elevation angle propagation measurements at L-band for land mobile satellite systems," *IEEE Trans. Veh. Technol.*, vol. 47, no. 3, pp. 1002–1011, Aug. 1998.

[17] C. Loo, "Land mobile satellite channel measurement at Ka band using Olympus," in *Proc. IEEE VTC' 94*, Stockholm, 1994, pp. 919–923.

[18] C. Loo, "Statistical models for land mobile and fixed satellite communications at Ka band," in *Proc. IEEE VTC' 96-spring*, Atlanta, GA, Apr. 1996, pp. 1023–1027.

[19] H.-P. Lin, R. Akturan and W. J. Vogel, "Photogrammetric satellite PCS channel modeling using Markov chain approach," in *Proc. IEEE ICC' 96*, Dallas, Jun. 1996, pp. 1735–1739.

[20] H. Suzuki, "A statistical model for urban radio propogation," *IEEE Trans. Commun.*, vol. 25, no. 7, pp. 673–680, Jul. 1977.

[21] C. Loo, "A statistical model for a land mobile satellite link," *IEEE Trans. Veh. Technol.*, vol. 34, no. 3, pp. 122–127, Aug. 1985.

[22] E. Lutz, D. Cygan, M. Dippold, F. Dolainsky, and W. Papke, "The land mobile satellite communication channel-recording, statistics, and channel model," *IEEE Trans. Veh. Technol.*, vol. 40, no. 2, pp. 375–386, May 1991.

[23] ITU-R P.525-3, "Calculation of free-space attenuation", Sept. 2016.

[24] ITU-R P.676-11, "Attenuation by atmospheric gases", Sept. 2016.

[25] ITU-R P.838-7, "Characteristics of precipitation for propagation modelling", Jun. 2017.

[26] ITU-R P.840-7, "Attenuation due to clouds and fog", Dec. 2017.

[27] ITU-R P.531-13, "Ionospheric propagation data and prediction methods required for the design of satellite services and systems", Sept. 2016.

[28] L. Bai, C.-X. Wang, J. Huang, Q. Xu, Y. Yang, G. Goussetis, J. Sun, and W. Zhang, "Predicting wireless mmWave massive MIMO channel characteristics using machine learning algorithms," *Wireless Commun. Mobile Computing*, vol. 2018, Article ID 9783863, https://doi.org/10.1155/2018/9783863, Aug. 2018.

[29] J. Huang, C.-X. Wang, L, Bai, J. Sun, Y. Yang, J. Li, O. Tirkkonen, and M. Zhou, "A big data enabled channel model for 5G wireless communication systems," *IEEE Trans. Big Data*, 2019, in press.

[30] S. Ventouras, *et al.*, "Large scale assessment of Ka/Q band atmospheric channel across Europe with ALPHASAT TDP5: The augmented network", in *Proc. IEEE EUCAP' 17*, Paris, France, Mar. 2017.

[31] Keras Document, https://keras.io/

[32] S. Ruder, "An overview of gradient descent optimization algorithms," *arXiv preprint arXiv:1609.04747v2*, 2016.

[33] X. Glorot and Y. Bengio, "Understanding the difficulty of training deep feedforward neural networks," *Journal of Machine Learning Research*, vol. 9, pp. 249–256, 2010.